PCCP

PAPER

View Article Online
View Journal | View Issue

Cite this: *Phys. Chem. Chem. Phys.*, 2017, **19**, 4114

A density functional theory based approach for predicting melting points of ionic liquids†‡

Lihua Chen[ab] and Vyacheslav S. Bryantsev*[b]

Accurate prediction of melting points of ILs is important both from the fundamental point of view and from the practical perspective for screening ILs with low melting points and broadening their utilization in a wider temperature range. In this work, we present an *ab initio* approach to calculate melting points of ILs with known crystal structures and illustrate its application for a series of 11 ILs containing imidazolium/pyrrolidinium cations and halide/polyatomic fluoro-containing anions. The melting point is determined as a temperature at which the Gibbs free energy of fusion is zero. The Gibbs free energy of fusion can be expressed through the use of the Born–Fajans–Haber cycle *via* the lattice free energy of forming a solid IL from gaseous phase ions and the sum of the solvation free energies of ions comprising IL. Dispersion-corrected density functional theory (DFT) involving (semi)local (PBE-D3) and hybrid exchange–correlation (HSE06-D3) functionals is applied to estimate the lattice enthalpy, entropy, and free energy. The ions solvation free energies are calculated with the SMD-generic-IL solvation model at the M06-2X/6-31+G(d) level of theory under standard conditions. The melting points of ILs computed with the HSE06-D3 functional are in good agreement with the experimental data, with a mean absolute error of 30.5 K and a mean relative error of 8.5%. The model is capable of accurately reproducing the trends in melting points upon variation of alkyl substituents in organic cations and replacement one anion by another. The results verify that the lattice energies of ILs containing polyatomic fluoro-containing anions can be approximated reasonably well using the volume-based thermodynamic approach. However, there is no correlation of the computed lattice energies with molecular volume for ILs containing halide anions. Moreover, entropies of solid ILs follow two different linear relationships with molecular volume for halides and polyatomic fluoro-containing anions. Continuous progress in predicting crystal structures of organic salts with halide anions will be a key factor for successful prediction of melting points with no prior knowledge of the crystal structure.

Received 8th December 2016,
Accepted 12th January 2017

DOI: 10.1039/c6cp08403f

www.rsc.org/pccp

1. Introduction

Ionic liquids (ILs) have been studies for use in organic synthesis, catalysis, separations, and electrochemical applications.[1,2] Such great interest in ILs is motivated by their unique physiochemical properties, including low melting points, negligible vapour pressure, high conductivity, and superior electrochemical and thermal stability.[1,2] In recent years, due to their excellent behaviour to induce extremely high charge densities at the interface with strongly correlated materials by a small applied bias, ILs have begun to serve as gate dielectrics of field effect transistors.[3–5] The extensive use of ILs promotes the development of novel ILs tailored to the specific application. However, due to many different combinations of organic cations and anions the number of potential ILs is huge. It is time and cost consuming to select an IL for the particular application with experimental methods. Therefore, developing theoretical methods that can accurately predict properties of ILs is essential for the accelerated discovery and rational design of new ILs with desirable properties.

[a] *Department of Materials Science and Engineering, University of Connecticut, Storrs, CT 06269, USA*

[b] *Chemical Sciences Division, Oak Ridge National Laboratory, Oak Ridge, TN 37831, USA. E-mail: bryantsevv@ornl.gov; Fax: +1-865-576-7956; Tel: +1-865-576-4272*

‡ Electronic supplementary information (ESI) available: Full details of computing ΔG_{latt}, a description of the computational protocol based on the VBT approach, Table S1 showing the comparison of the computed and experimental lattice parameters and molecular volumes for 11 ILs, Table S2 listing the lattice enthalpies, entropies, and free energies, solvation free energies, and the resulting fusion free energies at standard conditions, Fig. S1 showing a correlation of computed and experimental melting points, and Cartesian coordinates of all the polyatomic ions accompanied by their electronic energies obtained at the M06-2X/6-31+G(d, p) level of theory. See DOI: 10.1039/c6cp08403f

Low melting points enable the application of ionic liquids as solvents, electrolytes, and liquid gate dielectrics. For example, a bias driven formation of very thin electric double layers at the liquid/complex oxide interface at lower temperatures can allow the access to critical phase transition spaces that are currently inaccessible with traditional solid–solid field effect transistors.[3–5] Computer-aided screening of new ILs can play a critical role in significantly reducing the experimental effort to identify unique cation/anion combinations yielding ILs with low melting points. However, because of the complex influence of intermolecular forces on the stability of the solid and the liquid phase, melting points of ionic liquids are notoriously difficult to predict. While several methods with a varying degree of complexity, extent of parameterization, the range of applicability, and basis in fundamental thermodynamics have been proposed over the years for calculating the melting temperatures of ILs, according to Valderrama,[6] "it is a myth that, with the present experimental data and knowledge we have of ILs, we can obtain accurate and generalized correlations and estimation methods for determining melting temperatures of ILs".

Chemical homology, group contribution methods, quantitative structure–property relationship, and artificial neutral network[6–10] constitute a range of empirical methods available to estimate melting points of ILs. These models rely on the availability and accuracy of experimental melting temperatures for predefined types of ILs. The limits of applicability of such models depend on the size of the available experimental datasets, within which each model is developed. For example, in the framework of the group contribution method, additional cations are typically formed by adding methylene groups to parent cations, while each anion forms a separate group. This illustrates the limitation of the model to describe the properties of more exotic ILs incorporating a new cationic or anionic species.

Classical molecular dynamics (MD) simulations have been widely used to study the structural, thermodynamic, and transport properties of ILs,[11–17] although the melting points have been more difficult to predict.[16,18] The free energy based pseudo-supercritical path (PSCP) method, developed by Maginn and co-workers,[16] was shown to be the most reliable and robust approach for the computation of melting points of ILs. As with any classical MD simulation, one must be concerned about the availability and the quality of the available force field. While the predominant number of classical MD simulations of ILs employs pair-wise nonpolarizable potentials, it was shown by Borodin[18] that in order to provide an accurate description of both thermodynamic and transport properties of ILs, the many-body polarizable interactions should be included. By employing the nonpolarizable GAFF force field, the melting temperatures calculated with the PSCP method exhibited great sensitivity to three different methodologies used to estimate the atomic charges: the variation of 63 K in the case of $[C_4mim][PF_6]$ and 93 K in the case of $[C_2mim][PF_6]$.[19] *Ab initio* MD simulations can overcome some of the limitations of the empirical potential models, wherein polarization and charge transfer effects are treated implicitly. Currently, however, such simulations are restricted to a small number of ion pairs and short simulation times, which is insufficient to calculate quantities, such as melting temperature, *via* the free-energy based methods.

Direct calculations of the ion-pair binding energies and lattice energies have failed to rationalize the melting temperatures of ILs, raising the question whether the sole consideration of interaction energies is adequate to explain the melting process.[17,20,21] At the melting temperature the solid and liquid phase are in equilibrium, suggesting a simple thermodynamic approach to relate the Gibbs free energy of fusion from the solid to the molten phase to the melting temperature of IL. The approach for predicting melting temperatures of ILs based on the properties of isolated ions was developed by Krossing *et al.*[22] Enthalpy and entropy of an ionic lattice was deduced through correlations with the formula-unit volume of individual cations and anions using the volume-based thermodynamics (VBT) approach, originally formulated by Mallouk *et al.*[23] and further developed by Jenkins *et al.*[24,25] for inorganic salts. The approach has been applied for a set of 14 aprotic ionic liquids with known dielectric constants using the COSMO solvation model to determine single ion solvation free energies. The major limitation of the VBT method is that it only takes into account the long-range electrostatic interactions, but breaks down in the presence of specific interactions, such as the π–π stacking, hydrogen bonding, *etc.* For example, applying Krossing method[22] to protic ILs failed to yield any correlation with the experimental melting temperatures.[20] In the subsequent work,[26,27] the original approach was refined to treat a much broader selection of ILs *via* the introduction of additional molecular descriptors and presented in two formulations containing five and nine empirical parameters. The approach has proven to be useful in predicting melting points, but because it is based on the VBT approximation, it has not been extended for ILs containing strongly coordinated ions, such as halides and protic groups.

A different methodology for predicting melting temperatures based on the analysis of the potential energy surfaces (PESs) using the model of anharmonic oscillator for ion pairs of ILs was proposed by Zvereva *et al.*[28] This approach allowed the rationalization and correlation of melting temperatures with computed characteristics of PESs of ILs comprising ions that do not form strong and cooperative hydrogen bonds. However, it is not applicable for ILs containing halides, which cannot be regarded as consisting of distinct ion pairs.

A brief overview of several melting temperature prediction methods indicates that each of them has a limited range of applicability defined by the set of ILs used to parameterize the model and the necessity to have the experimental melting temperatures to obtain generalized correlations. To the best of the authors' knowledge, there have been no theoretical studies to estimate melting temperatures from lattice enthalpies, lattice entropies, and ion solvation free energies calculated directly using density functional theory (DFT) based methods. In what follows, we present a straightforward approach for predicting melting temperatures of ILs using a combination of the dispersion corrected generalized gradient approximation (GGA) PBE-D3[29] and hybrid HSE06-D3[30,31] exchange–correlation functionals for solid state calculations and a generic IL solvation model (SMD-GIL) of Cramer, Truhlar, and co-workers[32] for modeling

liquid phase thermodynamics. The important finding of this work is that with no empirical parameters, beyond those used in the underlying theoretical methods for the gas phase, solution phase, and solid state calculations, the best model is not only capable of capturing the trends in melting points upon variation of alkyl substituents in organic cations and anion species, but also well suited to provide estimation of the absolute melting points with accuracy comparable to that obtained with empirical and semiempirical prediction models. Being a purely theoretical melting temperature prediction method, it has a greater potential to be applicable for a wide range of ILs, but with the drawback of prior knowledge of the crystal structure. However, with the rapid advancement of the crystal structure prediction methods for organic compounds, we might expect a continuous progress in determining suitable starting crystal structure geometry based on purely the computed-aided structure elucidation.

2. Methodology

Here, we adopt a methodology based on the Born–Fajans–Haber cycle, originally developed by Krossing and co-workers,[22] in the context of the VBT method. The melting point (T_m) is determined as a temperature at which the solid and the liquid (molten) phase are in equilibrium, *i.e.*, the Gibbs free energy of fusion is zero, $\Delta G_{fus} = 0$. According to the Born–Fajans–Haber cycle shown in Fig. 1, ΔG_{fus} is given by

$$\Delta G_{fus} = -\Delta G_{latt} + \Delta G^{o\text{–}l}_{solv}, \quad (1)$$

where ΔG_{latt} is the lattice Gibbs free energy corresponding to forming the solid IL ($[C][A]_s$) from gaseous ions (C_g^+ and A_g^-) and $\Delta G^{o\text{–}l}_{solv}$ is the difference between the standard chemical potentials of C^+ and A^- in the gas phase and the liquid phase. ΔG_{latt} at a given temperature T and pressure P is defined as

$$\Delta G_{latt} = \Delta H_{latt} - T\Delta S_{latt}, \quad (2)$$

$$\Delta H_{latt} = \Delta U_{latt} + P\Delta V = \Delta U_{latt} - 2RT, \quad (3)$$

where ΔH_{latt}, ΔS_{latt}, ΔU_{latt} and ΔV are the lattice enthalpy, entropy, internal energy and volume change, respectively, and R is the ideal gas constant. The $P\Delta V$ term in the enthalpy for solids is generally negligible at ordinary pressures, whereas $P\Delta V = RT$ for each gaseous species, making up the $-2RT$ term in eqn (3). The lattice internal energy, ΔU_{latt}, can be written as a sum of two parts: the lattice potential energy, ΔU_0, and the internal thermal energy change, ΔU_{therm}, *i.e.*,

$$\Delta U_{latt} = \Delta U_0 + \Delta U_{therm}. \quad (4)$$

ΔU_0 can be expressed as

$$\Delta U_0 = \left(E^{[C][A]_s}_{total}/Z + E^{[C][A]_s}_{ZPE}/Z\right) - \left(E^{C_g^+}_{total} + E^{C_g^+}_{ZPE}\right) - \left(E^{A_g^-}_{total} + E^{A_g^-}_{ZPE}\right), \quad (5)$$

where E^X_{total} and E^X_{ZPE} (X = C_g^+, A_g^-, and $[C][A]_s$) are the total energies and zero-point vibrational energies of cations and anions in the gas phase and solids, respectively. Z is the number of formula units included in the unit cell. Likewise, ΔU_{therm} and ΔS_{latt} were estimated from the differences between the sum of the corresponding quantities of gas-phase ions and the solid phase using rigid-rotor harmonic-oscillator approximation.[33] All three translational, rotational, and vibrational contributions to the internal energy and entropy were included for the gas-phase ions, while only the vibrational contribution was considered for the solids. Additionally, three acoustic modes of solids were approximated by a $3RT$ term per ion at high temperature limit.[34] Full details of computing ΔG_{latt} are given in the ESI‡ section.

The right arm of Fig. 1, $\Delta G^{o\text{–}l}_{solv}$, can be written as

$$\Delta G^{o\text{–}l}_{solv} = \mu^l_{solv}([C][A]) - \mu^o_g(C^+) - \mu^o_g(A^-), \quad (6)$$

where $\mu^l_{solv}([C][A])$, $\mu^o_g(C^+)$, and $\mu^o_g(A^-)$ are the chemical potentials of $C^+$and A^- in the liquid and gas phase, respectively. This process corresponds to the free energy of transfer of ions from the gas phase at a concentration of 1 atm to the liquid phase at concentration of ions as in liquid IL. Therefore, $\Delta G^{o\text{–}l}_{solv}$ can be expressed as the sum of the solvation free energies of the constituent ions associated with the 1 mol L^{-1} (gas) → 1 mol L^{-1} (solution) process (ΔG^*_{solv}) and the standard state correction term ($\Delta G^{o\text{–}l}$) for each ion, *i.e.*,

$$\Delta G^{o-l} = \Delta G^*_{solv}(C^+) + \Delta G^*_{solv}(A^-) + 2\Delta G^{o-l}. \quad (7)$$

The latter term is the free energy change of 1 mol of an ideal gas from 1 atm (V^o = 24.46 L mol^{-1}) to molar ion concentration c ($V^l = 1/c$ L mol^{-1}) in liquid IL.

$$\Delta G^{o-l} = -T\Delta S^{o-l} = RT\ln\left(\frac{V^o}{V^l}\right) = RT\ln(24.46c) \quad (8)$$

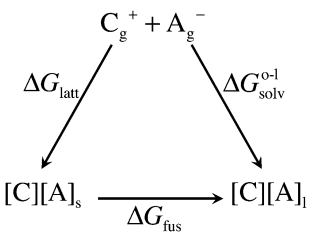

Fig. 1 The Born–Fajans–Haber cycle for the assessment of the fusion Gibbs free energy, ΔG_{fus}, from the lattice free energy, ΔG_{latt}, and the sum of the solvation free energies of the constituent ions, $\Delta G^{o\text{–}l}_{solv}$. C_g^+ and A_g^- are the gas-phase ions. A binary IL is denoted by $[C][A]_s$ and $[C][A]_l$ in the solid state and liquid form, respectively.

3. Computational methods

DFT calculations of the lattice Gibbs free energies were performed using the Vienna Ab-initio Simulation Package (VASP).[35–37] The valence electronic states were expanded on the basis of plane waves, and the core-valence interaction was described through the Projector Augmented Wave (PAW) approach. The Perdew–Burke–Ernzerhof (PBE)[29] generalized gradient approximation (GGA) functional and a plane wave kinetic energy cutoff of 1000 eV for the basis set were employed. For the bulk calculations, the Brillouin zone was sampled using a Monkhorst–Pack k-point

mesh of 2 × 2 × 2 for most ILs, resulting in less than 0.01 eV change in the total energy compared to 4 × 4 × 4. The *k*-point mesh of 1 was used for cell dimensions with the lattice constant larger than 15 Å. The two-body dispersion interactions in ILs were included using the DFT-D3 method of Grimme[38] implemented in VASP. Additionally, the single-point energy three-body dispersion term was computed using the DFT-D3 code.[39] The convergence threshold on forces for each atom was set to 0.01 eV $Å^{-1}$ and 0.005 eV $Å^{-1}$ in optimizing the solid and gas-phase structures, respectively. For charged systems, the leading monopole–monopole and quadrupole–monopole correction terms for the electrostatic interaction energy between the images of charged supercells were included.[40] Given the size of the unit cell (containing from 68 to 144 atoms), the phonon frequencies were calculated at the Gamma point only. Additionally, single-point energy calculations on the PBE-D3 optimized geometries were performed with the Heyd–Scuseria–Ernzerhof 06 (HSE06) hybrid functional,[38,41] which partially reduces the self-interaction error due to inclusion of the exact Hartree–Fock exchange and offers improved accuracy in describing the interaction between the charged fragments.[42,43] The computed ΔU_0 and ΔG_{fus} will be written with the superscripts PBE-D3 and HSE06-D3 to indicate the applied DFT method.

The solvation free energies of ions were computed using a generic IL SMD solvation model (SMD-GIL) of Cramer, Truhlar, and co-workers.[32] Using the gas-phase geometries, solvation calculations were performed at the M06-2X/6-31+G(d,p) level of theory, as implemented in Gaussian 09.[44] This model takes into account several macroscopic solvent descriptors that were averaged over 8 to 10 ILs, for which the experimental data are available. These solvent descriptors and their generic values are given as follows: the dielectric constant of solvent ($\varepsilon = 11.5$), the index of refraction ($n = 1.43$), the macroscopic surface tension ($\gamma = 61.24$ cal mol^{-1} $Å^{-2}$), and Abraham's hydrogen bond acidity $\left(\sum \alpha_2^H = 0.229\right)$ and basicity $\left(\sum \beta_2^H = 0.265\right)$ for the solvent when treated as a solute. The other two solvent descriptors are the fraction of non-hydrogen atoms that are aromatic carbon atoms (ϕ) and the fraction of non-hydrogen atoms that are electronegative halogen atoms (ψ). They are determined by the molecular structure of IL ions and for the ILs considered in this work are listed in Table 1. Using a generic set of parameters, the solvation free energies of 344 neutral solutes in 11 different ionic liquids were accurately estimated,[32] with a mean unsigned error of 0.43 kcal mol^{-1}. The choice of the atomic radii that determine the van der Waals envelope of the solute is critical for getting accurate results with implicit solvation models. Since the atomic radii for Cl and Br are optimized for neutral molecules, the computed solvation free energies of the halide ions could be underestimated. Indeed, the predicted difference in the solvation free energies between Cl^- and Br^- in a generic IL is 47.1 kJ mol^{-1}, which is significantly larger than the experimental difference between the two ions in two protic solvents, H_2O and CH_3OH, and two aprotic solvents, CH_3CN and DMSO.[45] To match the average experimental free energy difference of 12.6 kJ mol^{-1} for the two ions in aprotic solvents, we corrected the solvation free energy of Br^- by −34.5 kJ mol^{-1}.

Table 1 Structure dependent solvent descriptors adopted in the SMD-GIL solvation model. ϕ and ψ, respectively, are the fraction of non-hydrogen atoms that are aromatic carbon atoms and the fraction of non-hydrogen atoms that are electronegative halogen atoms

ILs	ϕ	ψ
$[C_1mim][Cl]$	0.375	0.125
$[C_2mim][Br]$	0.333	0.111
$[C_2mmim][Cl]$	0.300	0.100
$[C_2mmim][Br]$	0.300	0.100
$[C_2mim][BF_4]$	0.231	0.308
$[C_2mim][PF_6]$	0.200	0.400
$[C_4mim][Cl]$	0.273	0.091
$[C_3mim][PF_6]$	0.188	0.375
$[C_4mmim][Cl]$	0.250	0.083
$[C_4mmim][PF_6]$	0.167	0.333
$[C_1mpyr][Tf_2N]$	0.182	0.273

4. Results and discussion

4.1 Ionic liquids selection

A series of 11 ILs, Fig. 2, were selected for study based on several criteria. ILs were taken from a database[8] of 136 ILs that were carefully selected to assure reliable melting points. Searching the Cambridge Structural Database (CSD, 2016)[46] for this set of ILs with no error and no disorder yielded 21 structures. The number of structures was reduced to 13 by limiting the number of the atoms in the unit cell for the largest polymorph <150 and the length of the alkyl chain <6 carbon atoms. Finally, two $[C_nmim][MeSO_4]$ ILs were excluded from the initial analysis, because one of the members of a homologous series $[C_2mim][EtSO_4]$ has a dielectric constants of $\varepsilon = 35$[47] significantly different from the generic dielectric constant ($\varepsilon = 11.5$) employed in our work, which can cause a larger error in melting point prediction.[25] We will return to the question of sensitivity of the results to the dielectric constant change at the end of this section. The resulting 11 ILs contain three cation series: 1,3-dimethyimidazolium (C_nmim^+), 1,2,3-trimethyimidazolium (C_nmmim^+) and pyrrolidinium (C_nmpyr^+), where n is the number of carbon atoms in the alkyl chain. Together with these cations, the studied Ils contain two halide anions, Cl^- and Br^-, and three polyatomic fluoro-containing anions, PF_6^-, BF_4^-, and Tf_2N^-.

4.2 Crystal structures of ILs

Pictorial views of unit cells of ILs investigated in this work are shown in Fig. 2. In the case when several polymorphs exist, the structure with the lowest energy is given. The effect of inclusion the dispersion correction on the lattice parameters of ILs can be seen from Table 2, which shows the mean absolute error (MAE) and the mean relative error (MRE) with respect to experimental values. The performance of PBE and PBE-D3 for predicting the molecular volume, V_m, (unit cell volume per formula unit) for specific IL is also illustrated in Fig. 3. Other details involving lattice parameters for all ILs are provided in the ESI‡ section (Table S1). Comparison with the experimental data indicates that the PBE functional significantly overestimates the lattice parameters of ILs, with the relative error for V_m being 8–15%. In contrast, the PBE-D3 method on average slightly underestimates the lattice parameters, with the percent errors for V_m less than 4%.

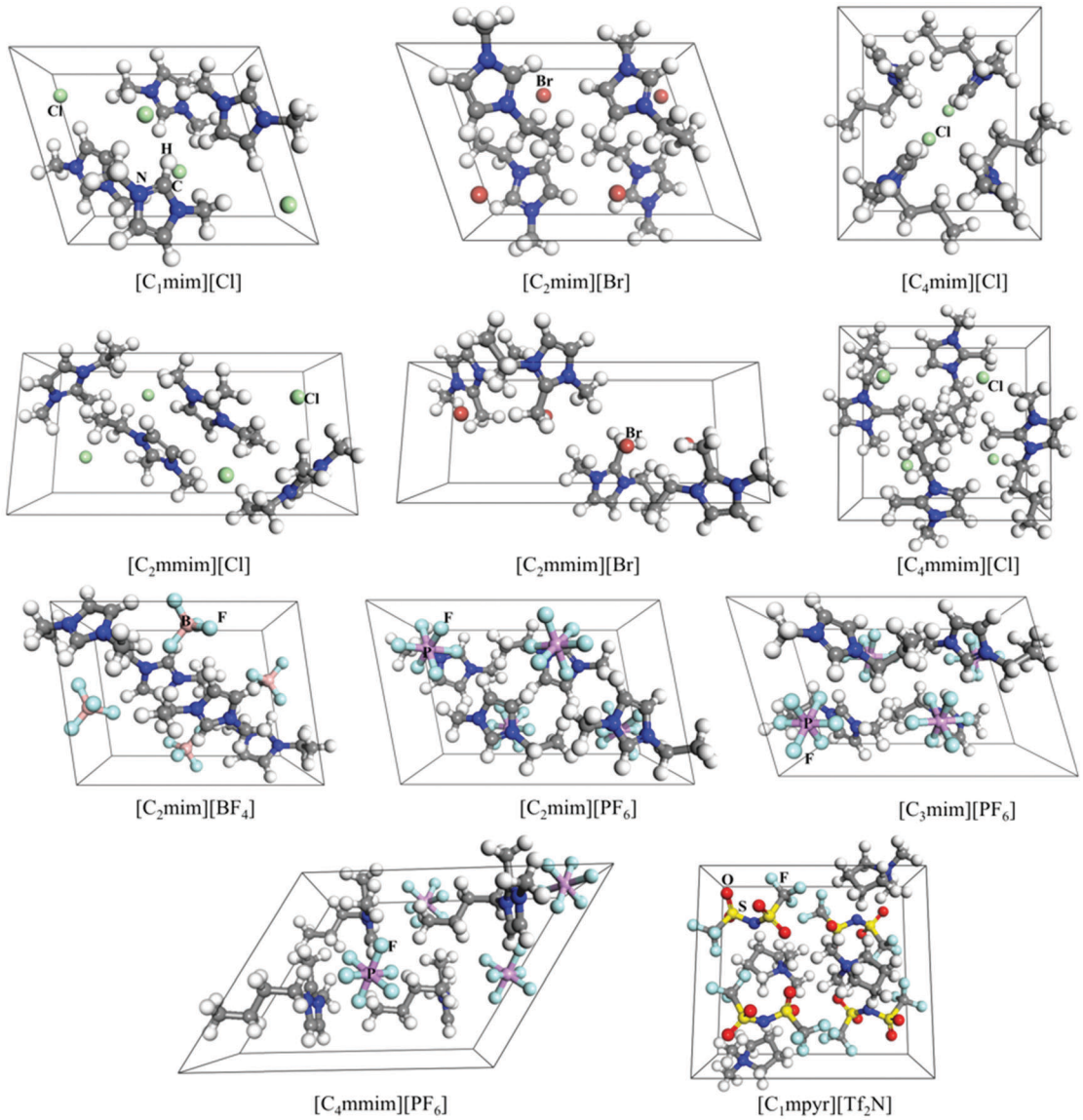

Schematic representations of the constituent ions of ILs above.

Cations:

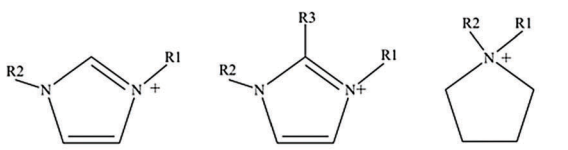

C_nmim^+ C_nmmim^+ C_1mpyr^+

R1=C_nH_{2n+1}, R2=CH_3 R1=C_nH_{2n+1}, R2=R3=CH_3 R1=R2=CH_3

Anions:

Cl^- Br^- BF_4^- PF_6^-

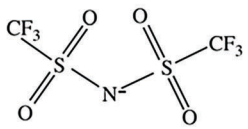

Tf_2N^-

Fig. 2 Perspective views of the crystal structures of selected ILs and the schematic representations of their constituent ions. The C, N, H, O, S, F, Cl and Br atoms are denoted by grey, blue, white, red, yellow, cyan, light-green, and brown colors, respectively.

Taking into account a small expansion of the lattice due to vibrations (by at most 2%), the agreement between the computational results using the PBE-D3 method and experiment is excellent. In addition to molecular volumes, we have also estimated the degree of similarity between the experimental and calculated crystal structures by superimposing these structures and calculating the root-mean-square deviation (RMSD) of the atomic displacements for the non-hydrogen atoms.

Table 2 The mean absolute error (MAE) and the mean relative error (MRE) of lattice parameters and molecular volumes, V_m for 11 ILs with respect to experimental values taken from the CSD database

	Lattice constants		Cell angle[a]		V_m	
Methods	MAE (Å)	MRE (%)	MAE (deg.)	MRE (%)	MAE (Å^3)	MRE (%)
PBE-D3	0.09	0.89	0.82	0.80	4.34	1.81
PBE	0.68	6.48	2.26	2.35	31.06	11.97

[a] The two cell angles are fixed at $\alpha = \beta = 90^\circ$.

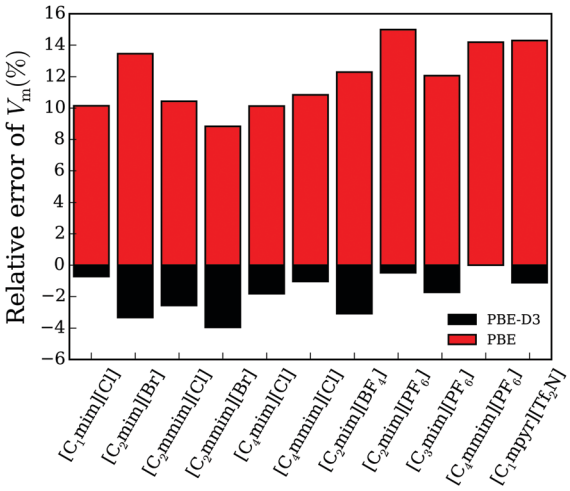

Fig. 3 The PBE and PBE-D3 relative errors of the molecular volume (V_m) for 11 ILs, denoted by red and black colors, respectively.

The PBE-D3 method (the mean RMSD of 0.13 Å) significantly outperforms the PBE method (the mean RMSD of 0.43 Å) in predicting the structural data, reinforcing the results obtained for the lattice constants and volumes. Therefore, the PBE-D3 method along with the HSE06-D3 single-point energies on PBE-D3 optimized geometries was applied for the subsequent evaluation of lattice enthalpies and entropies.

4.3 Lattice enthalpies, ΔH_{latt}

Lattice enthalpies have been determined by subtraction the sum of the enthalpies of the isolated ionic species from the enthalpy of the crystal lattice. As ILs are composed of oppositely charged ions, the electrostatic attraction is the dominant contribution to the net lattice energy. There has been a tremendous progress in predicting molecular crystals and ranking of polymorph composed of neutral molecules with dispersion-corrected GGA DFT.[31,48–50] However, because of the self-interaction error, GGA DFT tend to overdelocalize the charge, resulting in the fractional charge transfer for organic salts.[51,52] To alleviate this problem, we have used the HSE06-D3 functional, which includes a 25% fraction of exact exchange. A comparison of the net charges on each fragment using Bader analysis[53,54] (Table 3) indeed shows that ion charges are closer to the formal charge of ±1 with the HSE06-D3 functional. This leads to a higher electrostatic attraction and, consequently, to more negative ΔU_0 values obtained with the HSE06-D3 functional (on average by 12.6 kJ mol^{-1}) in comparison with the PBE-D3 functional. The results, Table 3, also emphasize the importance of the dispersion correction that can be 12–25% of $\Delta U_0^{HSE06\text{-}D3}$. As expected, the magnitude of the dispersion interaction increases with the number and length of the alkyl groups and the size of an anion.

In general, crystal structures of halide-based ILs exhibit much higher absolute ΔU_0 compared to the crystal structures containing a polyatomic fluoro-containing anion. These differences can be rationalized through combination of long-range and short-range interactions in the solid state. The long-range electrostatic interaction is determined by ion density and packing in the crystal lattice, which can be conveniently represented by the Madelung constant. With the EUGEN method[55] developed by Izgorodina and Macfarlane, the computed Madelung constants are in the range 1.39–1.50 for halide-based ILs and 1.10–1.30 for ILs with polyatomic anions, which can be compared with the value of 1.748 for NaCl. In addition to short-range van der Waals interactions present in all systems, halide anions with small size and high charge density are able to participate in relatively strong hydrogen-bonding interactions with the aromatic and alkyl C–H groups of the cationic species. This interaction is characterized by C–H$\cdots$halide contacts that are as short as 2.47 Å for Cl^- and 2.53 Å for Br^-.

Having calculated the lattice potential energies, ΔU_0, of ILs, it is instructive to examine if there is any correlation between ΔU_0 the molecular volume, V_m. A volume-based thermodynamic (VBT) approach has become a popular tool for predicting physical properties of ionic solids from molecular volumes or densities. A correlation between ΔU_0 and the inverse cube root of V_m, originally developed by Mallouk *et al.*[23] and expanded by Jenkins, Glasser, and co-workers,[22,24,25,56–58] for predicting thermodynamic data across an extended range of inorganic compounds, for 1 : 1 salts has the form

$$\Delta U_0 = 2(\alpha(V_m)^{-1/3} + \beta) \quad (9)$$

where α and β are empirically derived parameters. The same empirical model was applied for organic salts[56] and ILs,[57,58] but a subsequent comparison with the experimental ΔU_0 revealed the need for a specific parametrization of eqn (9) over a

Table 3 Net charges of anions from Bader population analysis and the lattice potential energy, ΔU_0, (kJ mol^{-1}) computed with the PBE-D3 and HSE06-D3 functionals. A dispersion correction (a sum of two- and three-body terms) obtained with the HSE06-D3 functional, E_{disp}, (kJ mol^{-1}) is also shown

	Net ion charge		ΔU_0		E_{disp}
ILs	PBE-D3	HSE06-D3	PBE-D3	HSE06-D3	HSE06-D3
[C$_1$mim][Cl]	−0.784	−0.813	−574.67	−587.67	−70.62
[C$_2$mim][Br]	−0.758	−0.792	−559.28	−568.67	−82.35
[C$_2$mmim][Cl]	−0.781	−0.810	−573.85	−599.40	−86.32
[C$_2$mmim][Br]	−0.747	−0.777	−556.21	−578.77	−85.86
[C$_4$mim][Cl]	−0.795	−0.823	−586.41	−591.13	−98.45
[C$_4$mmim][Cl]	−0.790	−0.819	−578.41	−586.53	−107.05
[C$_2$mim][BF$_4$]	−0.947	−0.966	−527.06	−536.32	−87.75
[C$_2$mim][PF$_6$]	−0.972	−0.987	−519.43	−529.47	−99.36
[C$_3$mim][PF$_6$]	−0.974	−0.988	−514.22	−527.34	−109.82
[C$_4$mmim][PF$_6$]	−0.976	−0.990	−513.58	−526.00	−123.84
[C$_1$mpyr][Tf$_2$N]	−0.956	−0.971	−505.76	−515.91	−126.97

different set of organic compounds. One possible explanations for a different set of empirical parameters needed for organic salts is that unlike inorganic 1 : 1 salts, the Madelung constant for organic salts can vary in a significant range (from 1.19 to 1.64), depending on the specific composition and arrangement of ions in the solid state. Moreover, as only the long-range electrostatic interactions were considered in the established correlations of Jenkins and Glasser, the omission of the short-range dispersion, π–π staking, and hydrogen bonding interactions could result in significantly underestimated ΔU_0 of ILs. A plot of computed ΔU_0 *versus* $(V_m)^{-1/3}$ shown in Fig. 4(a) reveals that only for ILs with a polyatomic anion there is a monotonic decrease in lattice potential energy with increasing volume, *e.g.*,

$$\Delta U_0^{\text{HSE06-D3}} = -71.76(V_m)^{-1/3} - 417.83, \qquad (10)$$

but any correlation of ΔU_0 with V_m for halide-based ILs is essentially nonexistent. Therefore, the VBT approach is expected to break down for ILs containing halides, requiring the use of more accurate and advanced DFT methods for this type of ILs.

4.4 Lattice entropies, ΔS_{latt}

To evaluate the lattice free energy, both enthalpic and entropic terms are needed. The formation of an ordered salt from gas-phase ions yields a substantial positive, destabilizing $T\Delta S_{\text{latt}}$ contribution, resulting in a substantially less negative ΔG_{latt} compared to ΔH_{latt}. As follows from Fig. 4(b), the lattice entropies, ΔS_{latt}, are only weakly dependent on T in the range of 200–500 K (<22 J mol^{-1} K^{-1}), but have a strong dependence on the composition of IL (from −330 to −440 J mol^{-1} K^{-1}). The least negative ΔS_{latt} for [C$_1$mim][Cl] and the most negative ΔS_{latt} for [C$_4$mmim][PF$_6$] are largely due to the logarithmic dependence of the translational entropy on the ion mass (to the power 3/2).

According to the volume-based entropy equation,[24,57] the absoluter entropies of solid materials vary linearly with molecular volume. Different empirical correlations were established for both ionic solids and organic liquid.[24] In the absence of more directly obtained parameters, the average values of the linear correlation constants for ionic solids and organic liquids were used to approximate the absolute entropies of ILs.[59] The standard absolute entropies of solid ILs, $S^{298.15}_{[C][A]_s}$, estimated at the Gamma point within the harmonic approximation are given in Fig. 4(c). Interestingly, the absolute entropies of ILs with the monatomic anion and the polyatomic anion follow different linear relations with molecular volume. Halide-based ILs held together by stronger interionic forces exhibit consistently smaller entropies. The results underscore that there are intrinsic differences within two groups of ILs that are not accounted for by the correlation with molecular volume alone. The fitted equations of absolute entropies (J mol^{-1} K^{-1}) with volume (in nm^3) at different temperatures take the form

$$S^{\text{monoatomic}}_{[C][A]_s} = 3.267TV_m + 175.8V_m - 0.1057T + 12.28, \quad R^2 = 0.996 \qquad (11)$$

$$S^{\text{polyatomic}}_{[C][A]_s} = 3.164TV_m + 300.2V_m - 0.0156T + 7.85, \quad R^2 = 0.997 \qquad (12)$$

where the superscripts following the S refer to the type of an anion. These equations might be applicable to other members of

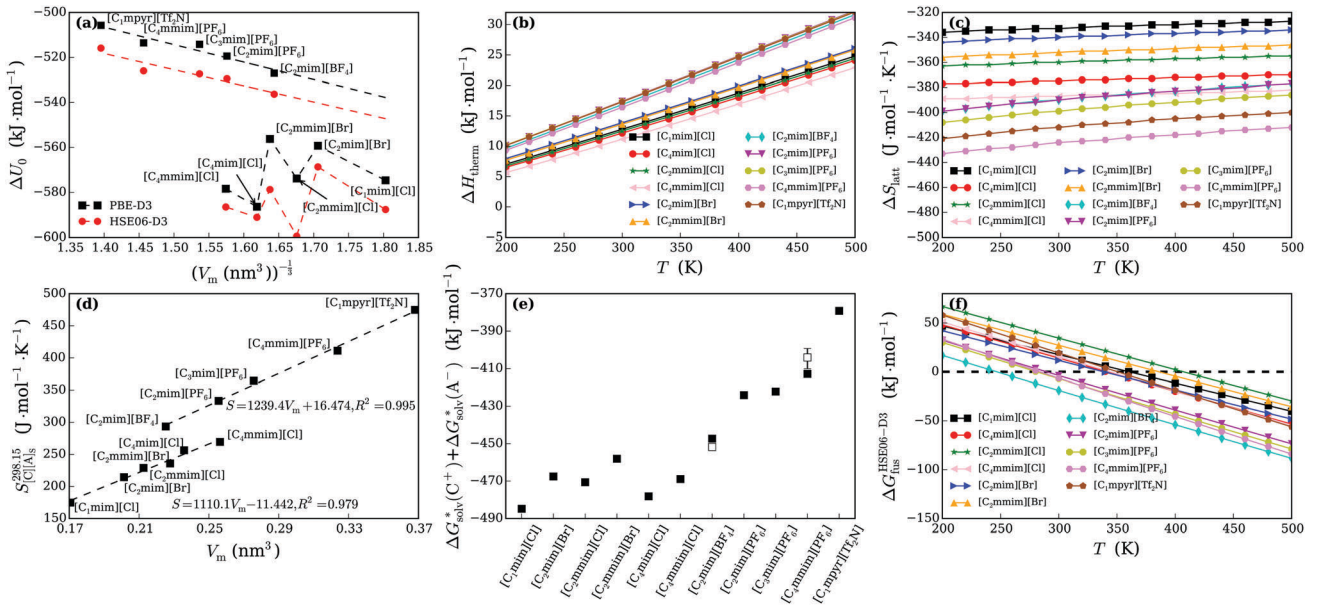

Fig. 4 (a) Plots of PBE-D3 and HSE06-D3 lattice potential energies, ΔU_0, *versus* $(V_m)^{-1/3}$; (b) plots of the thermal corrections to enthalpy, ΔH_{therm}, *versus* temperature, T; (c) plots of the lattice entropy, ΔS_{latt}, *versus* T; (d) plots of the standard absolute molar entropy of solid [C][A], $S^{298.15}_{[C][A]_s}$, *versus* molecular volume, V_m; (e) the sum of the solvation free energies of constituent ions of ILs, $\Delta G^*_{\text{solv}}(C^+) + \Delta G^*_{\text{solv}}(A^-)$, computed with the generic (ε = 11.50, solid squares) and experimental (empty squares) dielectric constants. The experimental dielectric constants are 12.8 for [C$_2$mim][BF$_4$] and 9.4 ± 1 for [C$_4$mmim][PF$_6$]; (f) plots of the HSE06-D3 fusion free energy, $\Delta G^{\text{HSE06-D3}}_{\text{fus}}$, *versus* temperature ($T$).

the family of ILs with halide and polyatomic fluorine-containing anions ILs series.

4.5 Solvation free energies, ΔG^{o-l}_{solv}

The right arm of the thermodynamic cycle depicted in Fig. 1, $C_g^+ + A_g^- \rightarrow [C][A]_l$, is associated with the difference in the chemical potentials of the two ions in the gas phase and in the IL. According to eqn (7), this process can be represented as the sum of ion solvation free energies, $\Delta G^*_{solv}(C^+) + \Delta G^*_{solv}(A^-)$, that are directly related to the solute–solvent interactions and the additional contribution, $\Delta G^{o-l} = RT\ln(24.46c)$, that accounts for the difference in the ion concentrations in two phases. The latter term can be estimated directly by expressing c, the molar concentration of ions in liquid IL, either in terms of the known density and molar mass or the known/predicted molecular volume. In the present work, it was approximated based on the experimental molecular volume in the solid state listed in Table 2. Due to a logarithmic dependence of free energy on c, only a rough estimate of c is needed. For example, consider $[C_2mim][BF_4]$, for which the difference of nearly 11% between the experimental (7.145 mol L^{-1})[60] and estimated (7.371 mol L^{-1}) molar concentration using the solid-state volume have resulted in the ΔG^{o-l} error of only 0.25 kJ mol^{-1} at T = 298.15 K.

The ion solvation free energies were estimated using a generic ionic liquid implicit solvation model, SMD-GIL,[32] developed for predicting free energies of solvation of organic solutes. Since the solvation model was fitted to reproduce the experimental data at standard conditions, only the solvation free energies at T = 298.15 K are available. This model can provide the upper and lower bound of $\Delta G^*_{solv}(C^+/A^-)$ at temperatures lower and higher than 298.15 K, respectively. The temperature dependence of the self-solvation free energy of a tight-ion-pair of IL can, in principle, be included in the framework of the statistical mechanical COSMO-RS approach[61,62] that will be the subject of future studies. Another limitation of the current model is the use of a generic dielectric constant ε = 11.5 averaged over 10 ILs. The effect of using a different ε when it is available for the IL under consideration on the predicted $\Delta G^*_{solv}(C^+/A^-)$ and melting temperatures will be discussed in the next section. The calculated sum of the solvation free energies of the two ions for each ionic liquid at 298.15 K is shown in Fig. 4(e). The large negative value of the free energy of solvation is what is expected for ILs formed by the combination of oppositely charged species. The results show two groupings of data, one for halide-containing ILs with stronger solvation and another for the polyatomic anion-containing ILs with weaker solvation. This is not surprising given a smaller size and a higher charge density of halides compared to bulkier BF_4^-, PF_6^-, and Tf_2N^- anions with delocalized electronic charge density.

4.6 Fusion free energies, ΔG_{fus}, and melting temperatures, T_m

An accurate prediction of the free energies of fusion, ΔG_{fus}, is far from straightforward, with errors arising from the offset of two large terms (see eqn (1)), the lattice free energy, $-\Delta G_{latt}$ and the solvation free energy, ΔG^{o-l}_{solv}. Therefore, it could be challenging to compute the absolute T_m values from ΔG_{fus}, with a predictable degree of accuracy using the approach embodied in Fig. 1 without a proper calibration of a theoretical model. Fig. 4(f) shows the variation of ΔG_{fus}, computed with the HSE06-D3 functional as a function of temperature T. As expected, ΔG_{fus} is positive at lower T and negative at higher T. The point at which ΔG_{fus} = 0 determines the melting temperature.

Table 4 provides a comparison of the predicted and the experimental melting temperatures of the studied ILs. The SMD-GIL solvation model at the M06-2X/6-31+G(d,p) level was used to calculate ΔG^{o-l}_{solv} and the two PBE-D3 and HSE06-D3 density functionals were employed to calculate ΔG_{latt}. Of these two approaches, the HSE06-D3 method is more accurate at predicting absolute melting points, with the MAE of 30.5 K and the MRE of 8.5%, as compared with 65.9 K and 18%, respectively, for the PBE-D3 calculations, with respect to the average experimental values.[8] The analysis of the results in Table 4 indicates that the HSE06-D3 method is very successful in predicting T_m for ILs the halide-based ILs, which are highly problematic for the VBT approach,[22–25,56,57] but the calculated T_m of ILs with polyatomic anions are systematically underestimated by an average of 35 K. This systematic deviation of the computed T_m could be due to deficiencies in the applied density functional theory, solvation model, or both. For example, adding a constant term of 10.8 kJ mol^{-1} to ΔG_{fus} can compensate a large part of the error, reducing the MAE and MRE to 13.9 K and 4.0%, respectively.

For ease of visualization, the performance of the HSE06-D3 method for predicting the melting temperatures of the studied ILs is presented in Fig. 5. A correlation of computed and experimental melting points is shown in the ESI‡ section (Fig. S1). Given various approximations, particularly the use of the polarizable dielectric continuum model in these calculations, the results demonstrate promising performance for a heterogeneous set of ILs. Several trends in computed T_m identified for a given set of ILs are fully consistent with the experimental data. Various contributions to ΔG_{fus} at T = 298.15 K that can help to

Table 4 Comparison of the computed melting temperatures (K) with the average experimental data collected in ref. 8. The lattice free energies are calculated using the PBE-D3 and HSE06-D3. The VBT results refer to the melting points predicted based on eqn (10)–(12). The mean absolute error (MAE) and the mean relative error (MRE) of each method with respect to the average experimental values are shown at the bottom

ILs	PBE-D3	HSE06-D3	VBT	Expt
$[C_1mim][Cl]$	316.04	361.06	264.39	399.45–398.15
$[C_4mim][Cl]$	327.76	341.77	198.68	343.15–314.10
$[C_2mmim][Cl]$	327.82	407.59	266.86	461.15
$[C_4mmim][Cl]$	321.53	344.70	209.74	372
$[C_2mim][Br]$	307.75	339.14	291.24	352.15–328.10
$[C_2mmim][Br]$	314.78	386.73	290.38	414.15
$[C_2mim][BF_4]$	219.27	245.94	285.37	288.15–279.15
$[C_2mim][PF_6]$	261.02	289.78	342.89	335.15–331.15
$[C_3mim][PF_6]$	244.64	281.15	321.98	313.15–294.15
$[C_4mmim][PF_6]$	251.75	283.77	318.63	313
$[C_1mpyr][Tf_2N]$	324.72	351.62	414.92	410.1–378.15
MAE (K)	65.94	30.49	77.25	
MRE (%)	17.99	8.47	19.99	

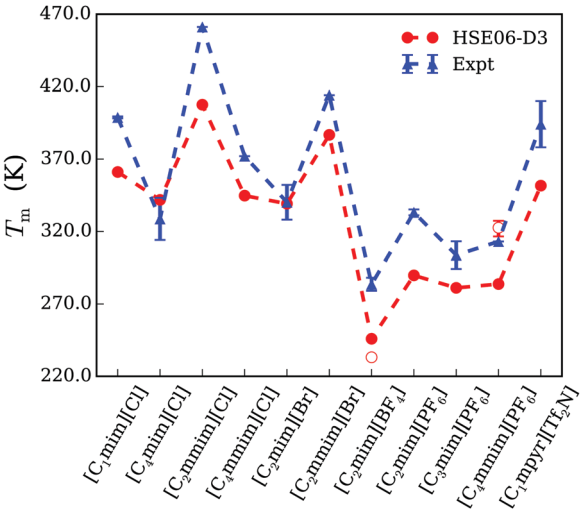

Fig. 5 Computed melting points from the HSE06-D3 functional and the experimental values obtained from ref. 8, denoted by red solid circle and blue triangle, respectively. The predicted melting points with experimental dielectric constants are marked with red empty circles.

rationalize the observed trends in T_m are listed in Table S2 of the ESI‡ section.

(i) A decrease in T_m with an increase in the alkyl chain length (n = 1–4) for ILs containing the imidazolium cation, *viz.* going from [C_1mim][Cl] to [C_4mim][Cl], from [C_2mmim][Cl] to [C_4mmim][Cl], and from [C_2mim][PF_6] to [C_3mim][PF_6]. This behavior can be attributed to a larger disruption of the interaction between the oppositely charged ions in the solid state than in the molten state as the alkyl chain length increases. For example, a small drop of 0.83 kJ mol^{-1} in $\Delta G^{o\text{–}l}_{solv}$ is overcompensated by a large drop of 20.73 kJ mol^{-1} in $-\Delta G_{latt}$ upon going from [C_2mmim][Cl] to [C_4mmim][Cl].

(ii) An increase in T_m with methylation at the C-2 position of imidazolium ring, *viz.* going from [C_2mim][Br] to [C_2mmim][Br] and from [C_4mim][Cl] to [C_4mmim][Cl]. Introduction of the methyl group at the C2-position results in weaker solvation that is not compensated by the change in the lattice free energy, which can become either less or more negative. For example, a large increase in T_m from [C_2mim][Br] to [C_2mmim][Br] is associated with a drop in $\Delta G^{o\text{–}l}_{solv}$ by 8.8 kJ mol^{-1} and a concomitant rise in $-\Delta G_{latt}$ by 7.8 kJ mol^{-1}.

(iii) A decrease in T_m by replacing halides with polyatomic anions, *e.g.*, going from [C_2mim][Br] to [C_2mim][PF_6] and [C_2mim][BF_4]. This trend can be interpreted in terms of a more dramatic decrease in the stability of the crystalline phase compared to the liquid phase as halides are replaced by larger anions. In addition to the lower lattice enthalpy, a larger increase in the entropy penalty for forming a crystal from isolated ions in the gas phase is also a contributing factor to a lower lattice free energy with polyatomic anions. Interestingly, comparing [C_2mim][PF_6] and [C_2mim][BF_4], the IL with the larger PF_6^- anion is not the one with the lower melting point. This is because of a much smaller ΔG^*_{solv} for a larger PF_6^- anion (−424.1 kJ mol^{-1}) over a smaller BF_4^- anion (−447.3 kJ mol^{-1}) that is not counterbalanced by the same degree of decrease in $-\Delta G_{latt}$, which is only 7.5 kJ mol^{-1}.

As follows from the foregoing discussion, the developed approach is quite successful at predicting melting points of ILs, but it is not without limitations. There is a question whether the polarizable dielectric continuum solvent model can capture the solvation thermodynamics in ILs. The SMD solvation was specifically parameterized for ILs and was applied successfully for predicting free energies of solvation of neutral solutes in ILs. Without any further modifications, except for the Br^- anion (see Section 3), this model has been used in the present work to calculate the solvation free energies of monovalent ionic solutes. A close agreement between the predicted and experimental melting points of ILs suggests reasonable description of ion solvation, at least on the relative basis over the range studied here. Including the ion pairs or larger aggregates explicitly is one possible strategy to improve the accuracy of solvation calculations for ions in ILs.

Since the necessary solvent parameters are often not available for a given IL, solvation calculations were carried out using the generic set of solvent-independent parameters, except for two descriptors that are fully determined by the molecular structure of IL ions (see Section 3). It is reasonable to assume that if solvent parameters are close to the average generic values than the performance of the solvation model by using either set of parameters will be similar. However, for ILs showing a large variation of parameters from the averaged values, it is anticipated that the variation in $\Delta G^*_{solv}(C^+/A^-)$ will be substantial. As the dielectric constant is one of the parameters greatly affecting the solvation free energy, we will illustrate the sensitivity of $\Delta G^{o\text{–}l}_{solv}$ and T_m to a change in ε by replacing the generic dielectric constant ε = 11.5 with the experimental ones. For example, taking ε_{expt} = 12.8 for [C_2mim][BF_4][63] results in a change by 4.4 kJ mol^{-1} to more negative $\Delta G^{o\text{–}l}_{solv}$ and 12.7 K to lower T_m. Conversely, taking ε_{expt} = 9.4 ± 1 for [C_4mmim][PF_6][47] produces a shift of 8.7 kJ mol^{-1} to less negative $\Delta G^{o\text{–}l}_{solv}$ and 22.6 K to higher T_m. While the resulting shifts in melting points are not outside the accuracy of the best computational method, the results do emphasize the importance of the prior knowledge of this parameter, if substantially greater variation in ε_{expt} is expected. Because of a relatively large ε_{expt} = 35 for [C_2mim][$EtSO_4$],[47] we have excluded ILs containing the $MeSO_4^-$ anion from our initial analysis (Section 4.1). For example, we find that with the generic value of ε = 11.5 the predicted melting points of [C_1mim][$MeSO_4$] is overestimated by a large margin, 87.5 K. However, when ε = 35 is employed, the error in the melting point prediction (2.8 K) becomes comparable to that observed for the other ILs. In the future work, we will investigate if combining quantum chemical gas-phase calculations for ion pairs with predictions of vapor pressure of ILs using the COSMO-RS approach[61,62] could realistically describe the interaction of ions with IL medium and make accurate predictions of T_m with no additional experimental input, such as dielectric constant.

Table 4 also lists the melting points calculated using the VBT approach, as described elsewhere.[22] A description of the computational protocol based on eqn (10)–(12) is provided in

the ESI‡ section. The results verify that the VBT approach is only applicable for ILs containing spherical or large polyatomic anion, but fails completely for ILs containing halide anions. Therefore, we had to rely on the existing crystal structures for making the assessment of the lattice free energy for halide-containing ILs. Since information on crystal structure is not available for the majority of ILs, the proposed protocol is not yet suitable for high-throughput prediction of melting points. However, with a fast pace of progress in developing *in silico* tools for crystal structure prediction of organic materials given only the structural formula, we expect the successful prediction of the lowest energy polymorphs for the unit cell size considered in this work can soon become feasible.

In this work we have tested the efficacy of one of the evolutionary methods, USPEX, developed by Oganov and co-workers[64–66] for crystal structure prediction. [C_1mim][Cl] was chosen based on the smallest unit cell containing 68 atoms. With USPEX input of 4 ion pairs, unit cell parameters 5% larger than experimental values, completely random orientation of ions and random space group, and the number of 40 structures in each generation, the calculations were set up to run up to 30 generations (a total 1200 structure optimizations). Although the experimental crystal structure was not found, the best-computed structure was only 4 kJ mol^{-1} higher in energy (per ion pair) than the experimental structure. This difference in energy results in the error of the computed melting point of only 13.85 K, which is within the predictive accuracy of the best model. However, the method can quickly become prohibitively expensive as the system size increases due to increasing cost of DFT calculations and the exponential grows of the number of local minima. Nevertheless, with the rapid development of the efficient algorithms for crystal structure prediction and the DFT methods for accurate ranking of the likely polymorphs, as well as increasing computer power, crystal structure prediction with >100 atoms in the unit cell could become more affordable in the near future.

5. Conclusions

Significant research efforts are directed toward the identification of ILs with the extended low temperature window of the liquid range desirable for various applications. However, a reliable prediction of melting points remains a difficult challenge. In this work, we have established a computational protocol for the prediction of melting points of ILs by evaluating the stability of ILs in the crystalline and molten states using density functional theory. The stabilization of ions in the periodic lattice and the molten state was calculated using the plane-wave based periodic DFT and the SMD-generic-IL solvation model, respectively. The most reliable prediction of melting points was obtained using the HSE06 hybrid functional augmented with the DFT-D3 dispersion correction term. The mean absolute error is 30.5 K and the mean relative error is 8.5% for 11 ILs consisting of imidazolium or pyrrolidinium cations and halide or polyatomic fluoro-containing anions. The results verify that this method is capable of quantitatively reproducing the variations in melting points by changing the length of the alkyl groups on the cation and replacing one anion by another. The proposed method is essentially parameter-free beyond the approximations made for computing lattice free energies and ion solvation free energies. Therefore, it has the advantage over the other approaches for the estimation of melting points of ILs reported in the literature in that it is not limited to the types of ions considered in this work and potentially applicable to a wide range of ILs.

The results of this work emphasize that unlike ILs containing spherical or large anions, the lattice energy of which can be approximated using the volume-based thermodynamic approach, prior knowledge of crystal structure is required to make accurate determination of the latticed energy for IL containing halide anions. The use of the generic dielectric constants in the SMD-generic-IL model implies that if the actual dielectric constant is significantly different from the generic value, it is preferred that the experimental dielectric constant is used whenever available to obtain more reliable predictions. With the development of crystal structure prediction algorithms and more accurate description of ion solvation in IL medium by including ion pairs or larger aggregates explicitly in the quantum chemical model, we might expect continuous progress towards fully *ab initio* prediction of melting points for a wide range of ILs with no experimental input.

Acknowledgements

This work was funded by the Laboratory Directed Research and Development Program of Oak Ridge National Laboratory, managed by UT-Battelle, LLC, for the U.S. Department of Energy. We are thankful to Vinit Sharma (ORNL) for making helpful suggestions. This research used resources of the National Energy Research Scientific Computing Center, a DOE Office of Science User Facility supported by the Office of Science of the U.S. Department of Energy under Contract No. DE-AC02-05CH11231.

References

1 P. Wasserscheid and T. Welton, *Ionic liquids in synthesis*, Wiley Online Library, 2008, vol. 1.
2 T. Welton, *Chem. Rev.*, 1999, **99**, 2071–2084.
3 T. Fujimoto and K. Awaga, *Phys. Chem. Chem. Phys.*, 2013, **15**, 8983–9006.
4 Y. Yamada, K. Ueno, T. Fukumura, H. Yuan, H. Shimotani, Y. Iwasa, L. Gu, S. Tsukimoto, Y. Ikuhara and M. Kawasaki, *Science*, 2011, **332**, 1065–1067.
5 A. C. Lang, J. D. Sloppy, H. Ghassemi, R. C. Devlin, R. J. Sichel-Tissot, J.-C. Idrobo, S. J. May and M. L. Taheri, *ACS Appl. Mater. Interfaces*, 2014, **6**, 17018–17023.
6 J. O. Valderrama, *Ind. Eng. Chem. Res.*, 2014, **53**, 1004–1014.
7 J. A. Lazzús, *Fluid Phase Equilib.*, 2012, **313**, 1–6.
8 C. L. Aguirre, L. A. Cisternas and J. O. Valderrama, *Int. J. Thermophys.*, 2012, **33**, 34–46.
9 A. R. Katritzky, A. Lomaka, R. Petrukhin, R. Jain, M. Karelson, A. E. Visser and R. D. Rogers, *J. Chem. Inf. Comput. Sci.*, 2002, **42**, 71–74.

10 A. Varnek, N. Kireeva, I. V. Tetko, I. I. Baskin and V. P. Solov'ev, *J. Chem. Inf. Model.*, 2007, **47**, 1111–1122.
11 M. L. S. Batista, J. A. P. Coutinho and J. R. B. Gomes, *Curr. Phys. Chem.*, 2014, **4**, 151–172.
12 T. Yan, C. J. Burnham, M. G. Del Pópolo and G. A. Voth, *J. Phys. Chem. B*, 2004, **108**, 11877–11881.
13 T. Köddermann, D. Paschek and R. Ludwig, *Curr. Phys. Chem.*, 2007, **8**, 2464–2470.
14 E. J. Maginn, *Acc. Chem. Res.*, 2007, **40**, 1200–1207.
15 M. S. Kelkar, W. Shi and E. J. Maginn, *Ind. Eng. Chem. Res.*, 2008, **47**, 9115–9126.
16 Y. Zhang and E. J. Maginn, *J. Chem. Phys.*, 2012, **136**, 144116.
17 E. I. Izgorodina, D. Golze, R. Maganti, V. Armel, M. Taige, T. J. Schubert and D. R. MacFarlane, *Phys. Chem. Chem. Phys.*, 2014, **16**, 7209–7221.
18 O. Borodin, *J. Phys. Chem. B*, 2009, **113**, 11463–11478.
19 Y. Zhang and E. J. Maginn, *J. Phys. Chem. B*, 2012, **116**, 10036–10048.
20 H. Markusson, J.-P. Belières, P. Johansson, C. Austen Angell and P. Jacobsson, *J. Phys. Chem. A*, 2007, **111**(35), 8717–8723.
21 U. L. Bernard, E. I. Izgorodina and D. R. MacFarlane, *J. Phys. Chem. C*, 2010, **114**, 20472–20478.
22 I. Krossing, J. M. Slattery, C. Daguenet, P. J. Dyson, A. Oleinikova and H. Weingärtner, *J. Am. Chem. Soc.*, 2006, **128**, 13427–13434.
23 T. E. Mallouk, G. L. Rosenthal, G. Mueller, R. Brusasco and N. Bartlett, *Inorg. Chem.*, 1984, **23**, 3167–3173.
24 H. D. B. Jenkins, H. K. Roobottom, J. Passmore and L. Glasser, *Inorg. Chem.*, 1999, **38**, 3609–3620.
25 H. D. B. Jenkins and L. Glasser, *Inorg. Chem.*, 2003, **42**, 8702–8708.
26 U. Preiss, S. Bulut and I. Krossing, *J. Phys. Chem. B*, 2010, **114**(34), 11133–11140.
27 U. P. Preiss, W. Beichel, A. M. Erle, Y. U. Paulechka and I. Krossing, *ChemPhysChem*, 2011, **12**(16), 2959–2972.
28 E. E. Zvereva, S. A. Katsyuba and P. J. Dysonb, *Phys. Chem. Chem. Phys.*, 2010, **12**, 13780–13787.
29 J. P. Perdew, K. Burke and M. Ernzerhof, *Phys. Rev. Lett.*, 1996, **77**, 3865–3868.
30 J. Heyd and G. E. Scuseria, *J. Chem. Phys.*, 2004, **121**, 1187–1192.
31 J. Heyd, J. E. Peralta, G. E. Scuseria and R. L. Martin, *J. Chem. Phys.*, 2005, **123**, 174101.
32 V. S. Bernales, A. V. Marenich, R. Contreras, C. J. Cramer and D. G. Truhlar, *J. Phys. Chem. B*, 2012, **116**, 9122–9129.
33 D. A. McQuarrie, and J. D. Simon, *Molecular thermodynamics*, University Science Books, Sausalito, CA, 1999.
34 H. Donald and B. Jenkins, *J. Chem. Educ.*, 2005, **82**, 950–952.
35 G. Kresse, *Ab initio* molekular dynamik für flüssige metalle, PhD thesis, Technische Universität Wien, 1993.
36 G. Kresse and J. Furthmüller, *J. Comput. Mater. Sci.*, 1996, **6**, 15–50.
37 G. Kresse and J. Furthmüller, *Phys. Rev. B: Condens. Matter Mater. Phys.*, 1996, **54**, 11169–11186.
38 S. Grimme, J. Antony, S. Ehrlich and H. Krieg, *J. Chem. Phys.*, 2010, **132**, 154104.
39 http://www.thch.uni-bonn.de/tc/index.php? section=downloads&subsection=DFT-D3&lang=english.
40 G. Makov and M. C. Payne, *Phys. Rev. B: Condens. Matter Mater. Phys.*, 1995, **51**, 4014–4022.
41 J. Moellmann and S. Grimme, *J. Phys. Chem. C*, 2014, **118**, 7615–7621.
42 J. G. Brandenburg, T. Maas and S. Grimme, *J. Chem. Phys.*, 2015, **142**, 124104.
43 V. L. Chevrier, S. P. Ong, R. Armiento, M. K. Y. Chan and G. Ceder, *Phys. Rev. B: Condens. Matter Mater. Phys.*, 2010, **82**, 075122.
44 M. Frisch, G. Trucks, H. B. Schlegel, G. Scuseria, M. Robb, J. Cheeseman, G. Scalmani, V. Barone, B. Mennucci, and G. E. Petersson, *et al.*, *Gaussian 09*, 2009.
45 C. P. Kelly, Christopher J. Cramer and D. G. Truhlar, *J. Phys. Chem. B*, 2007, **111**, 408–422.
46 C. R. Groom, I. J. Bruno, M. P. Lightfoot and S. C. Ward, *Acta Crystallogr.*, 2016, **72**, 171–179.
47 M.-M. Huang, Y. Jiang, P. Sasisanker, G. W. Driver and H. Weingärtner, *J. Chem. Eng. Data*, 2011, **56**, 1494–1499.
48 D. C. Sorescu, E. F. C. Byrd, B. M. Rice and K. D. Jordan, *J. Chem. Theory Comput.*, 2014, **10**, 4982–4994.
49 S. Zahn and B. Kirchner, *J. Phys. Chem. A*, 2008, **112**(36), 8430–8435.
50 M. G. Del Pópolo, C. Pinilla and P. Ballone, *J. Chem. Phys.*, 2007, **126**, 144705.
51 http://schooner.chem.dal.ca/downloads/talks/2015-scp.pdf.
52 A. J. Cohen, P. Mori-Sanchez and W. Yang, *Chem. Rev.*, 2012, **112**, 289–320.
53 G. Henkelman, A. Arnaldsson and H. Jónsson, *Comput. Mater. Sci.*, 2006, **36**, 254–360.
54 R. F. Bader, *Atoms in molecules*, John Wiley & Sons, Ltd, 1990.
55 E. I. Izgorodina, U. L. Bernard, P. M. Dean, J. M. Pringle and D. R. MacFarlane, *Cryst. Growth Des.*, 2009, **9**, 4834–4839.
56 K. E. Gutowski, J. D. Holbrey, R. D. Rogers and D. A. Dixon, *J. Phys. Chem. B*, 2005, **109**, 23196–23208.
57 L. Glasser, *Thermochim. Acta*, 2004, **421**, 87–93.
58 L. Glasser and H. D. B. Jenkins, *Phys. Chem. Chem. Phys.*, 2016, **18**, 21226–21240.
59 L. Glasser and H. D. B. Jenkins, *Thermochim. Acta*, 2004, **414**, 125–130.
60 O. Hiroyuki, *Electrochemical aspects of ionic liquids*, John Wiley & Sons, 2011.
61 A. Klamt, *Wiley Interdiscip. Rev.: Comput. Mol. Sci.*, 2011, **1**, 699–709.
62 M. Diedenhofen, A. Klamt, K. Marsh and A. Schäfer, *Phys. Chem. Chem. Phys.*, 2007, **9**, 4653–4656.
63 C. Wakai, A. Oleinikova, M. Ott and H. Weingaertner, *J. Phys. Chem. B*, 2005, **109**, 17028–17030.
64 A. R. Oganov and C. W. Glass, *J. Chem. Phys.*, 2006, **124**, 244704.
65 A. O. Lyakhov, A. R. Oganov, H. T. Stokes and Q. Zhu, *Comput. Phys. Commun.*, 2013, **184**, 1172–1182.
66 A. R. Oganov, A. O. Lyakhov and M. Valle, *Acc. Chem. Res.*, 2011, **44**, 227–237.

